The Muon g-2 in the Standard Model and Beyond

HE397: The Standard Model of Particle Physics

Balasubramanian A.A.G.; Kundu A.; Schwarze L.

April 15, 2025

Centre for High Energy Physics, IISc

Contents

Contents

Theoretical Framework

Introduction

- In non-relativistic quantum mechanics, the coupling of a particle spin to an electromagnetic background field is

$$H_I = g\mu\vec{B}\cdot\vec{S}$$

- μ is the Bohr magneton which is ($c = \hbar = 1$)

$$\mu = \frac{q}{2m}$$

- g is called the $g-$factor, forming the (intrinsic) **magnetic dipole moment** of a particle together with μ and $\vec{S}$

$$\vec{\mu} = g\mu\vec{S}$$

- The Dirac equation predicts $g = 2$ for fermions.
- This corresponds to the tree-level prediction of the standard model of particle physics (SM)

Introduction

How does $g = 2$ arise from the Dirac equation?

- The originally formulated Dirac equation with minimal coupling is

$$i\partial_t \psi = \left[\vec{\alpha}\left(\hat{p} - q\vec{A}\right) + q\varphi + \beta m\right]\psi$$

- $\psi = \psi(\vec{x}, t)$ is a four-component spinor

$$\psi(\vec{x}, t) = \begin{pmatrix} \tilde{\phi}(\vec{x}, t) \\ \tilde{\chi}(\vec{x}, t) \end{pmatrix}$$

- If the kinetic and electromagnetic energies are negligible compare to m, a WKB-type Ansatz suggests

$$\psi(\vec{x}, t) = \begin{pmatrix} \phi(\vec{x}, t) \\ \chi(\vec{x}, t) \end{pmatrix} \exp\left(-imt\right)$$

Introduction

How does $g = 2$ arise from the Dirac equation?

- dropping the subleading terms $\partial_t \chi(\vec{x}, t)$ and $q\varphi\chi$ then yields

$$\chi(\vec{x}, t) = \vec{\sigma} \cdot (\hat{p} - q\vec{A}) \frac{\phi(\vec{x}, t)}{2m},$$

  decoupling the equations

- The equation for ϕ may then be massaged to yield

$$i\partial_t \phi = \left[\frac{\left(\hat{p} - e\vec{A}\right)^2}{2m} - \frac{q}{m} \frac{\vec{\sigma}}{2} \cdot \vec{B} + e\varphi \right] \phi$$

- Together with μ and $\vec{S} = \frac{\vec{\sigma}}{2}$ this results in $g = 2$ for any spin-$1/2$ particle

Field Theoretic Framework

- The Dirac equation comes from the Lagrangian $\mathcal{L}_{\text{free}} = \bar{\psi}\left(i\not{D} - m\right)\psi$
- The Clifford algebra $\mathrm{Cl}\,(1,3)$ allows for 5 independent spinor bilinears

$$\bar{\psi}\psi \quad \bar{\psi}i\gamma^5\psi \quad \bar{\psi}\gamma^\mu\psi \quad \bar{\psi}\gamma^\mu\gamma^5\psi \quad \bar{\psi}\sigma^{\mu\nu}\psi$$

  with $\sigma^{\mu\nu} = \frac{i}{2}\left[\gamma^\mu, \gamma^\nu\right]$
- Bilinears 1 and 3 are already present in the Lagrangian
- Bilinears 2 and 4 are pseudoscalar and pseudovector terms
- The last term is of particular interest:

$$\sigma^{\mu\nu}F_{\mu\nu} = -2\begin{pmatrix} \left(\vec{B} + i\vec{E}\right)\cdot\vec{\sigma} & \\ & \left(\vec{B} - i\vec{E}\right)\cdot\vec{\sigma} \end{pmatrix}$$

  generating the desired $\psi - \vec{B}$ coupling

Field Theoretic Framework

- That $\mathcal{L}_{\text{free}}$ already includes $g = 2$ may be understood in terms of the **Gordon identity** on the amplitude level
- With this, the tree-level amplitude already contains the term

$$\mathcal{M}_0^\mu \supset -\frac{iq}{2m}\bar{u}q_\nu\sigma^{\mu\nu}u$$

  where q_ν is the momentum transfer (photon momentum)
- Therefore, any additional term of this kind generates a deviation to the classical $g = 2$ prediction
- Such terms may be generated through loop diagrams
- The quantity of interest is then the **vertex function** Γ^μ in the desired order of perturbation theory

QED

- To assess perturbative effects on the magnetic moment in pure QED one has to examine general vertices of the form

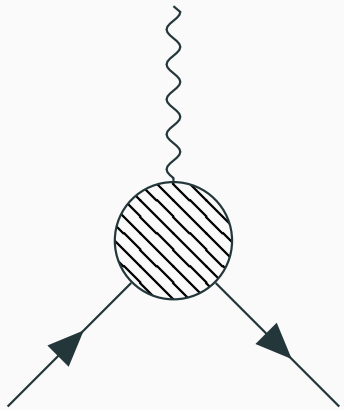

- The matrix element for a generalized (QED) vertex can be written as

$$\bar{u}(p_2)\left(f_1\gamma^\mu + f_2 p_1^\mu + f_3 p_2^\mu + f_4\sigma^{\mu\nu}p_{1\nu} + f_5\sigma^{\mu\nu}p_{2\nu}\right)u(p_1)$$

- Where momentum conservation was used to eliminate q. Current conservation $q_\mu\Gamma^\mu = 0$ (Ward Identity) gives $f_2 = f_3$ and $f_4 = -f_5$
- Since the external particles are on-shell and we have momentum conservation, we can say that the form factors only depend on $\frac{q^2}{m^2}$

QED

- Using the Gordon identity, we obtain the general form of the Matrix element up to arbitrary orders

$$i\mathcal{M}^{\mu} = (-ie)\bar{u}(p_2)\left[F_1\left(\frac{q^2}{m^2}\right)\gamma^{\mu} + \frac{i\sigma^{\mu\nu}q_{\nu}}{2m}F_2\left(\frac{q^2}{m^2}\right)\right]u(p_1)$$

- Thus, we have the g—factor $g = 2 + 2F_2(0)$
- Here, we define the magnetic anomaly

$$a \equiv \frac{g-2}{2} = F_2(0)$$

- We learn that vectorial spinor bilinears can be dropped when extracting $F_2(0)$
- Since the $\sigma^{\mu\nu}$ tensor structure is not present in the classical Lagrangian, one loop results will not contain divergences in F_2

QED

- There is only one NLO QED contribution to the magnetic moment

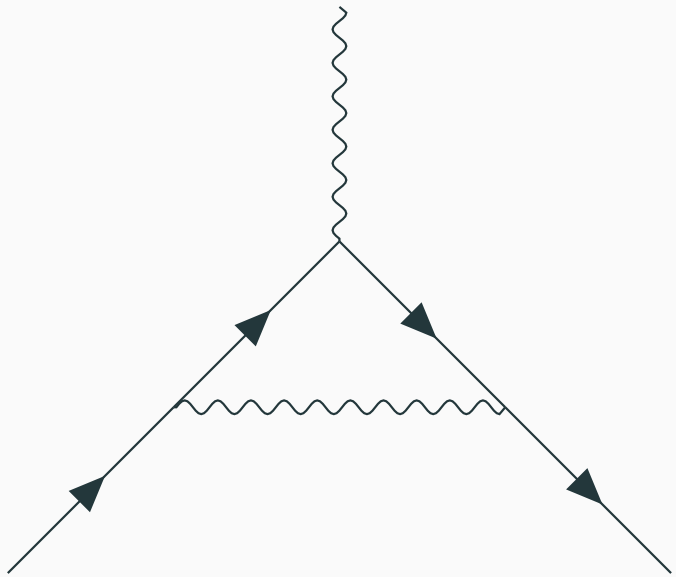

- Wave function renormalisation cannot form the desired tensor structure
- Instead, such vacuum polarisation diagrams contribute to the form factor F_1
- This diagram has been evaluated by Schwinger and results in $a = \frac{\alpha}{2\pi}$

QED

- Reproducing this result by hand is possible but quite involved
- Instead, this process is useful to learn how computational techniques can be used to compute such diagrams
- This approach lets us handle more complicated theories and higher loop orders in a much quicker way

- $\rightarrow$ `Mathematica`

Weak Currents and the Higgs

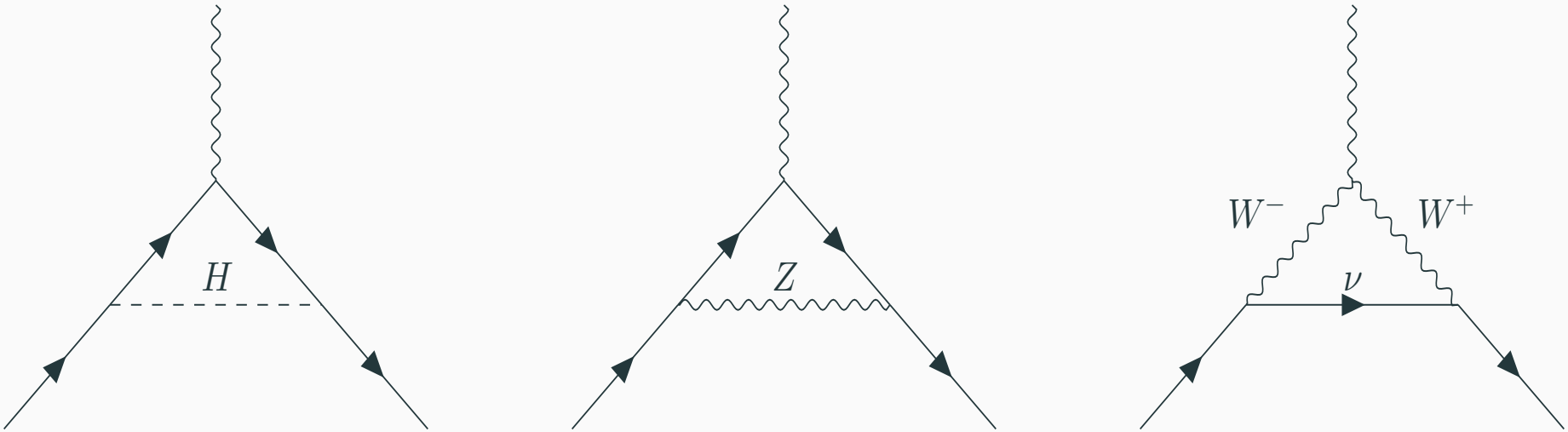

- There are three NLO contributions from weak currents and the Higgs sector
- In principle, these can be evaluated in analogy to pure QED
- However, the chiral structure of the electroweak theory allows for all spinor bilinears
- Here, one finds that $\bar{u}\gamma^{\mu}u$, $\bar{u}\gamma^{5}u$ and $\bar{u}\gamma^{\mu}\gamma^{5}u$ are not contributing to the magnetic moment
- The relevant term is the vector coupling to $\sigma^{\mu\nu}$

Weak Currents and the Higgs

- One needs to be even more careful
- In general gauges, the EW Goldstone modes may not be fully absorbed by the gauge bosons
- Diagrams involving the Goldstones can be necessary for keeping gauge invariance, especially on the computer
- Standard tools like FeynArts operate in R_ξ gauge by default
- At higher orders, Ghosts contributions arise

The Fruit of Labour

- Many physicists have contributed to the theoretical prediction of magnetic moment calculations in QED and weak theory
- The pure QED prediction accounts for over 99% of a_μ, the anomalous moment of the muon
- Up to **five loops**, the theoretical result is [Aoyama et al., 2012]

$$a_\mu^{\mathrm{QED}} = 116584718.931(104) \times 10^{-11}$$

- For weak currents and the Higgs, a two-loop 0.1 ppm result is sufficient for the current experimental accuracy [Gnendiger et al., 2013]

$$a_\mu^{\mathrm{Weak}} = 153.6(1.0) \times 10^{-11}$$

Beyond Electroweak Theory

- The magnetic moment of fermions can be predicted with astonishing theoretical accuracy
- The question arises if we missed anything – and what the consequences would be
- For one, we know that the SM is an effective field theory

How does new physics contribute?

Beyond Electroweak Theory

- Misinterpreted electric dipole moments shift observations of a_μ [Jegerlehner and Nyffeler, 2009]

$$\rightarrow d_\mu < \mathcal{O}\left(10^{-19} e \cdot \mathrm{c}m\right)$$

- New gauge bosons can modify the QED vertex at higher orders [Hooper et al., 2023]
- Dark photons can shift the magnetic moment of the leptons [Evans, 2024]
- Many Composite Higgs theories can accommodate partner particles that mix with the SM fermions [Xu and Zheng, 2022]
- Superpartners in SUSY models generate new loop contributions [Chakraborti et al., 2021]

The list continues almost endlessly

Beyond Electroweak Theory

- Many BSM models allow for tweaking parameters to accommodate large deviations to experiments
- However, the higher the experimental precision, the stronger are the bounds that can be put on BSM models
- $g-2$ is no exception. Even if potential deviations to the experiment vanish with higher experimental or theoretical accuracy, models that predict unfortunate shifts in magnetic moments can be restricted

However, before getting too excited with the endless possible modifications of magnetic moments in BSM physics, we should first fully investigate the SM. Hadronic contributions, which we so far swept under the carpet, will also contribute to the magnetic moment of fermions.

Experiments

Why Muon

- Our experiments for calculating the anomaly in the magnetic moment requires a lepton, but that gives us six choices: the three massive leptons e, μ and τ, and their corresponding neutrinos.
- Experimentally, it is quite hard to produce and detect any interactions with neutrinos, so that reduces the realistic candidates to three.
- The electron is the lightest lepton and is hence stable with no kinematic option for decay due to lepton number conservation.
- The τ lepton is quite heavy at 1.78 GeV, but the large mass allows for many different pathways for decay, along with a very short lifetime.
- Hence, the best candidate is the μ, which has an appreciably long lifespan ($\simeq 2.2\mu s$), which can be increased via boosts. Another convenient fact is that it has one majorly dominant pathway: $e\bar{\nu}_e\nu_\mu$, streamlining experimental design.

Larmor and Cyclotron Frequency

- In muon rest frame: $\mathcal{H}_{int} = -\vec{\mu} \cdot \vec{B}$, with $\vec{\mu} = \frac{e g_\mu}{2 m_\mu} \vec{s}$. For this case, we have the Larmor precession frequency as:

$$\vec{\omega_L} = \frac{g_\mu e}{2m} \vec{B}$$

- Similarly, from the Lorentz Force equation, we can derive the cyclotron frequency as:

$$\omega_c = \frac{e}{m\gamma} B$$

- But, we need to add a correction for the Thomas precession due to the centripetal force the muon beam faces in the storage ring, which is given by:

$$\vec{\omega_T} = \frac{\gamma^2}{\gamma + 1} \frac{\vec{a} \wedge \vec{v}}{c^2} \equiv (1 - \gamma) \frac{e}{m\gamma} \vec{B}$$

Anomalous precession frequency

Therefore, we have the anomalous precession frequency ω_a, the angular velocity of the μ wrt. the momentum, or mathematically, $\omega_L - \omega_c$ [Jegerlehner, 2017]:

$$\vec{\omega}_L = \frac{e}{m}\left[\left(\frac{g}{2} - 1 + \frac{1}{\gamma}\right)\vec{B} - \left(\frac{g}{2} - 1\right)\frac{\gamma\vec{\beta}}{\gamma+1}(\vec{\beta}\cdot\vec{B}) - \left(\frac{g}{2} - \frac{\gamma}{\gamma+1}\right)\frac{\vec{\beta}\wedge\vec{E}}{c}\right]$$

$$\vec{\omega}_c = \frac{e}{m}\left[\frac{1}{\gamma}\vec{B} - \frac{\gamma}{\gamma^2-1}\cdot\frac{\vec{\beta}\wedge\vec{E}}{c}\right]$$

$$\vec{\omega_a} = \frac{e}{m}\left[a_\mu\vec{B} - a_\mu\frac{\gamma}{1+\gamma}(\vec{\beta}\cdot\vec{B})\vec{B} - \left(a_\mu - \frac{1}{\gamma^2-1}\right)\frac{\vec{\beta}\times\vec{E}}{c}\right]$$

“Magic” Momentum of the Muon

- The extremely complicated general form of the anomalous precession velocity depends on the boost parameter and the orientation of the magnetic field.
- Putting $\vec{\beta} \cdot \vec{B} = 0$: motion perpendicular to the field - takes care of the second term.
- While we don’t know the exact value of a_μ, we have an excellent estimate for it- theoretically and experimentally.
- Putting a value of $\gamma = \sqrt{1 + \frac{1}{a_\mu}} \simeq 29.3$ gives us a momentum of 3.094 GeV, with a 10% uncertainty, at which the third term is highly suppressed, thus giving us back a close estimate of the value of the anomaly at zero momentum: which is otherwise experimentally impossible to attain due to breakdown of perturbation theory.

Muon Production and Decay channel

- Since the first experiments on muons, we have used the pion decay as a steady source for muon production: a proton beam bombarded on a target (basic processes $p + p \to p + n + \pi^+$ and $p + n \to p + p + \pi^-$) produces copious amounts of charged pions.
- Due to their low masses, only the muon and electron channels are kinematically allowed, with the low-mass lepton being heavily suppressed.
- In the weak decay, the positively charged leptons would be preferentially emitted with right-handed helicity. However, this is vetoed by the massless neutrino and by the conservation of angular momentum (the pion has zero spin).
- Since the pions are the lightest hadrons, the favoured decay channel is electroweak, thus making sure the muons are longitudinally polarized due to P violation.

Contd.: Pion Decay

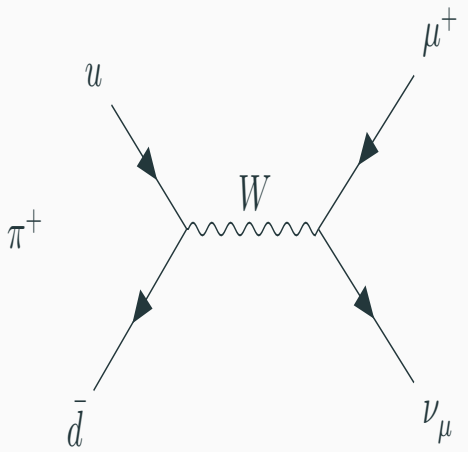

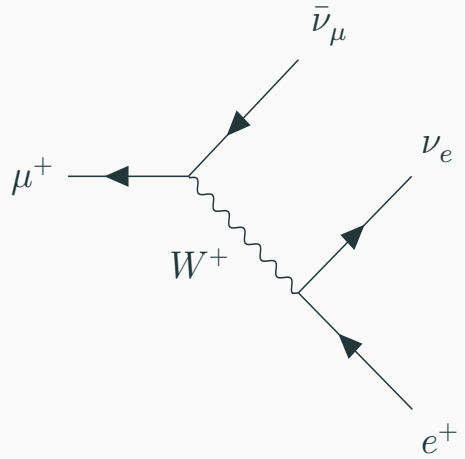

- The effective Fermi interaction for this process is :

$$\mathcal{L}_{\text{eff,int}} = -\frac{G_\mu}{\sqrt{2}} V_{ud} \left(\bar{\mu}\gamma^\alpha(1-\gamma_5)\nu_\mu\right)\left(\bar{u}\gamma_\alpha(1-\gamma_5)d\right) + \text{h.c.}$$

- Pion decay is a parity-violating weak decay where leptons of definite handedness are produced depending on the given charge. Thus, we end up with only one possibility Cotrozzi [2024] :

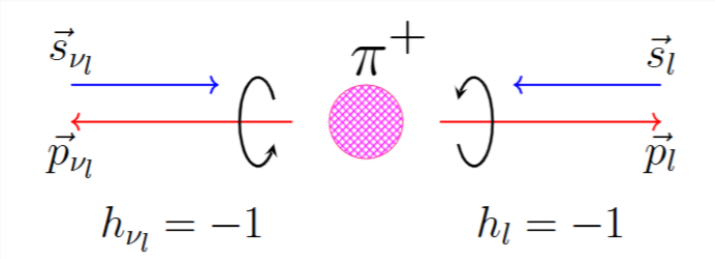

Contd.: Muon Decay

- Muon decay channel:

$$\mu^+ \to e^+ \nu_e \bar{\nu_\mu}$$

- Note: The differential decay width takes its maximum value for the highest energy positron whose momentum is parallel to the muon polarization: once again, this is a result of the parity violation of the V-A nature of weak decay, which prefers to couple to a right-handed positron (or a left-handed electron for a muon jet).
- Again, the effective Lagrangian reads:

$$\mathcal{L}_{\text{eff,int}} = -\frac{G_\mu}{\sqrt{2}} \left(\bar{e}\gamma^\alpha(1-\gamma_5)\nu_e\right)\left(\bar{\nu}_\mu\gamma_\alpha(1-\gamma_5)\mu\right) + \text{h.c.}$$

Contd.: Muon Decay

- The polarized differential decay probability to find an electron with energy between E and E+dE emitted at an angle between θ and $\theta + d\theta$ ($Q = p_\mu - p_e$, $Q^2 = m_\mu^2 + m_e^2 - 2(p_\mu \cdot p_e)$; $n_\mu = (0, P_\mu)$ in muon rest frame):

$$\frac{\mathrm{d}^2\Gamma}{\mathrm{d}E_e \mathrm{d}\cos\theta} = \frac{G_\mu^2}{12\pi^3}\frac{p_e}{E_\mu}\left\{Q^2(p_\mu p_e) + 2(Qp_\mu)(Qp_e) - (n_\mu p_e)\left(Q^2 - 2(Qp_e)\right)\right\}$$

- In terms of x = E/W, x_0 = m_e/W, where W = $(m_\mu^2 + m_e^2)/2m_\mu$:

$$\frac{d^2\Gamma^\pm}{dx\, d\cos\theta} = \frac{G_\mu^2 m_\mu^5}{192\pi^3}x^2\left(3 - 2x \pm P_\mu(2x-1)\cos\theta\right) = \tau_\mu^{-1}\frac{N(E)}{2}\left[1 + A(E)\cos\theta\right]$$

- Now considering the boosts, we get:

$$A(E) = P_\mu\left(\frac{x(2x-1)}{3+x-x^2}\right) \quad ; \quad N(E) \propto (x-1)^2(3+x-x^2)$$

The First Experiment

- Garwin, Lederman and Weinrich [Garwin et al., 1957] used a positively charged pion beam of 85 MeV stopped in a carbon absorber and a carbon target to stop the polarized muons emitted from pion decay.
- They then measured the positron count corrected against the background magnetic field with a scintillating telescope under the principle that a stronger magnetic field would imply a higher Larmor frequency of the muon before the decay.
- The plot showed P and C violation in muon decay, and the peak separation for the positron count gave the first measurement of the muon g-factor with a 10% precision, which wasn't enough to observe the magnetic anomaly.

The First Experiment Contd.

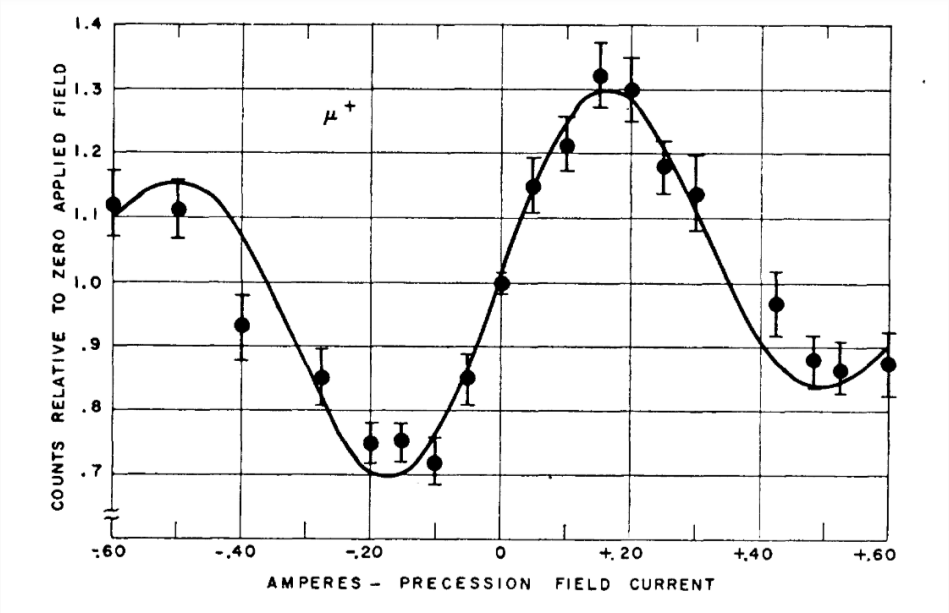

Figure 1: The plot of the number of events versus the magnetic field for a specific detector angular position [Garwin et al., 1957]

Experimental Data collection

Observables: $\omega_a = a_\mu \frac{qB}{m}$ (defined earlier, calculated through wiggle plot extrapolation); $\omega_p = 2\mu_p B$ (Larmor precession frequency of the protons in water).

$$a_\mu = \frac{\omega_a}{\omega_p} \frac{\mu_p}{\mu_e} \frac{m_\mu}{m_e} \frac{g_e}{2}$$

The other quantities are experimentally well-known constants obtained up to an overall certainty of $\simeq$ 25 ppb:

- μ_p: magnetic moment of free proton: 2.79284734462(82) μ_N [Schneider et al., 2017]
- μ_e: magnetic moment of free electron: -1.00115965218059(13) μ_B [Fan et al., 2023]
- g_e: g factor for electron: 0.00115965218059(13) [Fan et al., 2023]
- m_e: mass of electron: 0.5109895069(16) MeV [Navas et al., 2024]
- m_μ: mass of muon: 105.6583755(23) MeV [Navas et al., 2024]

Wiggle Plots

The number of positrons detected above a certain threshold E_{th} is given by a function: (N_0 and A are experimental parameters obtained by plot-fitting)

$$N(t) = N_0(E_{th})e^{-t/\gamma\tau}(1 + A(E_{th})cos(\omega_a t + \phi))$$

Meanwhile, statistical uncertainty $\delta\omega_a$ is expressed as [Jegerlehner, 2017]:

$$\frac{\delta\omega_a}{\omega_a} = \frac{\sqrt{2}}{\omega_a\gamma\tau A\langle P\rangle\sqrt{N}}$$

Where $\sqrt{N}$ is due to statistical deviation, A is due to $N^{-1}\partial N/\partial\omega_a \propto A$, the factor $\sqrt{2}/\omega_a\gamma\tau$ accounts for improvement of the accuracy with the number of oscillations, $\langle P\rangle$ is due to polarization. To minimize the statistical uncertainty of ω_a, the energy threshold is chosen such that the product NA^2 is maximized.

Wiggle Plots Contd.

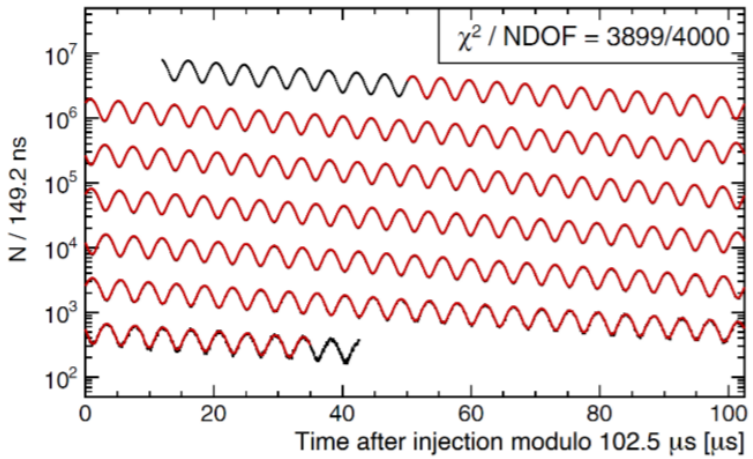

(a) Run-1 T-method wiggle plot.

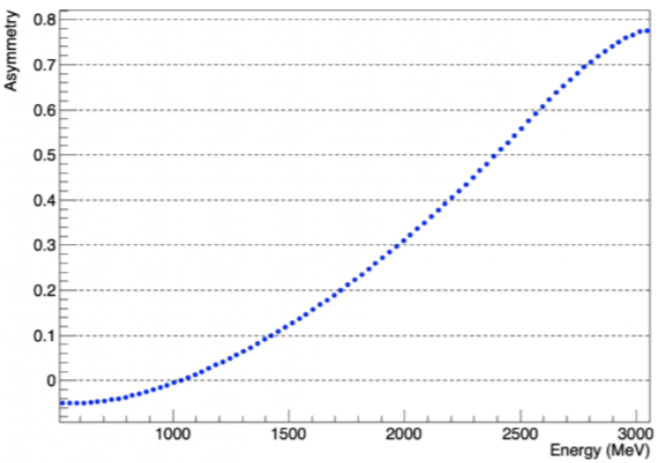

(b) A-Method energy weights.

- Threshold Method or T-Method: all positron events are integrated for energy above a fixed threshold, with equal weights (p(E) = 1). For this method, it was found that the statistical uncertainty is minimal if we integrate energies above 1.7 GeV.
- Asymmetry Weighted Method or A-Method: each positron event is weighted with the asymmetry function A(E) as a function of the positron energy. This technique yields the maximum statistical power, lowering the optimal energy threshold to 1 GeV.

Early Experiments: CERN I

- Experimental Setup: Protons were accelerated in the 600-MeV synchro-cyclotron, scattered against a beryllium target and produced pions; a positively charged muon beam was thus produced from pion decays.
- CERN I aimed to reach 1% accuracy on the anomaly since the theoretical QED corrections had already reached second order ($\simeq$0.001165). The final result showed good agreement with the theory:

$$a_{\mu}^{exp}(\text{CERN I}) = 0.001162(5) \rightarrow \pm 4300\text{ppm}$$

CERN I Contd.

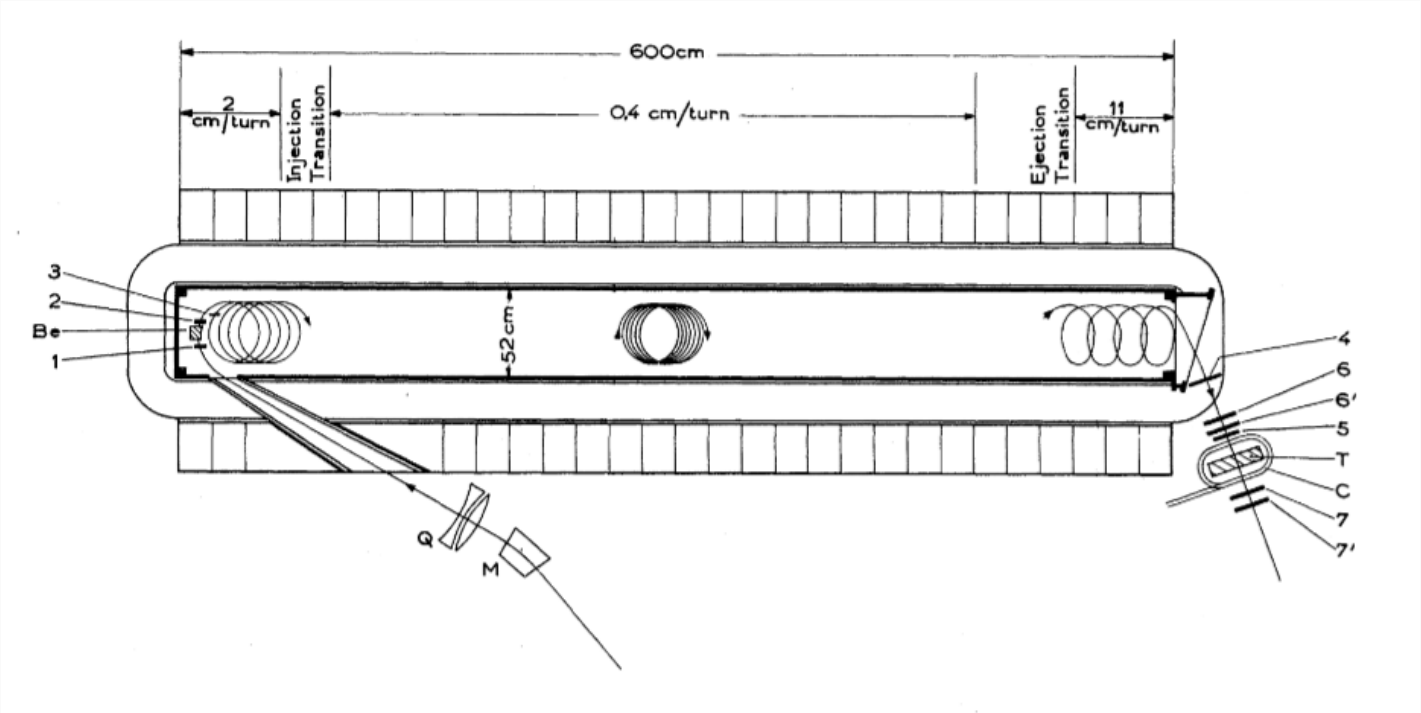

Figure 2: Overview of the CERN I experimental setup: an anti-muon beam was injected in the dipole magnet, and the coincidence of 1, 2 and 3 counters defined the injection signal; ejected muons stopped in target T, where the stop signal was a coincidence of counters 4, 5, 6, 6‘ and a veto on counter 7; after the stop signal, the coincidence of 6 – 6‘ or 7 – 7‘ defined forward and backwards emitted positrons

[Charpak et al., 1961]

Early Experiments: CERN II

Improvements:

- Storage Ring with a diameter of 5m for a 10.5 GeV proton beam
- Higher Luminosity from the Proton Synchrotron (which made up for protons that did not hit the target and pions that had not decayed, creating a large background (namely, the hadronic flash) and did not allow for an optimal initial muon polarization)
- The final results showed [Bailey et al., 1968]:

$$a_\mu^{exp}(\text{CERN II}) = 0.00116616(31) \rightarrow \pm 270\text{ppm}$$

which showed a deviation of 1.8σ from the theoretical estimate, but this was reconciled with sixth-order QED corrections.

Early Experiments: CERN III

Improvements:

- A Storage Ring with a diameter of 14 m was built and immersed in a 1.5 T dipole magnet field, with the beam target moved outside of the Ring so that the hadronic flash could be greatly reduced.
- Magic momentum $|p| = 3.09$GeV, greatly reducing the uncertainty in the calculations and boosting the mean lifetime of the muons to 64.4μs.
- The final result was mostly dominated by statistical errors and was precise enough for three-loop QED corrections and hadronic corrections [Bailey et al., 1975]:

$$a_{\mu^+}^{exp}(\text{CERN III}) = 0.001165911(11) \rightarrow \pm 9\text{ppm}$$
$$a_{\mu^-}^{exp}(\text{CERN III}) = 0.001165937(12) \rightarrow \pm 10\text{ppm}$$
$$a_{\mu}^{exp}(\text{CERN III}) = 0.001165924(8.5) \rightarrow \pm 7.3\text{ppm}$$

CERN III Contd.

The dilated lifetime allowed a huge dataset collection, so CERN III could verify the CPT theorem, which implies a_{μ^+} and a_{μ^-} should be equal. The experimental value, with 95% CL, was [Bailey et al., 1975]:

$$\frac{a_{\mu^+} - a_{\mu^-}}{a_\mu} \in [-50, 6] \times 10^{-6}$$

BNL data will later support this conclusion, with a much lower uncertainty owing to the larger sample size.

E821 Experiment @Brookhaven

Improvements over CERN III:

- Higher rate of muons: reaching a statistics 20 times as large as for CERN III, which was possible because the muon flux could be increased by approximately a factor of 400 thanks to the high luminosity of AGS (Alternating Gradient Synchrotron).
- A better way of injection: in CERN III, pions were injected in the ring and completed one orbit before impacting the exterior wall of the inflector. Thus muons emitted by pions were limited in number; in BNL, pions were allowed to decay in a long ($\simeq$ 80 m) channel upstream of the storage ring, and then the muon beam was directly injected into the ring.
- The storage ring with a diameter of 7 m was composed of three continuously wound superconductors instead of the 40 independent bending magnets of CERN III, which allowed the magnetic field to be much more uniform.

E821 Contd.

The final results for BNL were [Bennett et al., 2006]:

$$a_{\mu^+}^{exp}(\text{BNL}) = 0.0011659204(9) \rightarrow \pm 0.73\text{ppm}$$
$$a_{\mu^-}^{exp}(\text{BNL}) = 0.0011659214(9) \rightarrow \pm 0.72\text{ppm}$$
$$a_{\mu}^{exp}(\text{BNL}) = 0.00116592080(63) \rightarrow \pm 0.54\text{ppm}$$

The data had a deviation from the then theoretical value that included 5-loop QED calculations and the second-order of EW and hadronic loops: $a_\mu^{exp}(\text{BNL}) - a_\mu^{th} = 268.6(72.4) \times 10^{-11} \simeq 3.7\sigma$, implying BSM contributions.

E989 Experiment @Fermilab

Improvements:

- The average rate of muon injection was 12 Hz, compared to only 4.4 Hz at BNL, allowing a much larger dataset for calculation.
- A longer pion decay line ($\simeq$ 2 km), ensuring a highly reduced hadronic flash from pion decay to neutrons.
- A high precision laser calibration system to continuously re-calibrate the detectors, which reduces systematic error on ω_a.
- Hardware upgrades (Edge shims, wedge shims, top hats and steel foils) to increase the magnetic field uniformity by a factor of 3 wrt. BNL.

E989 Contd.

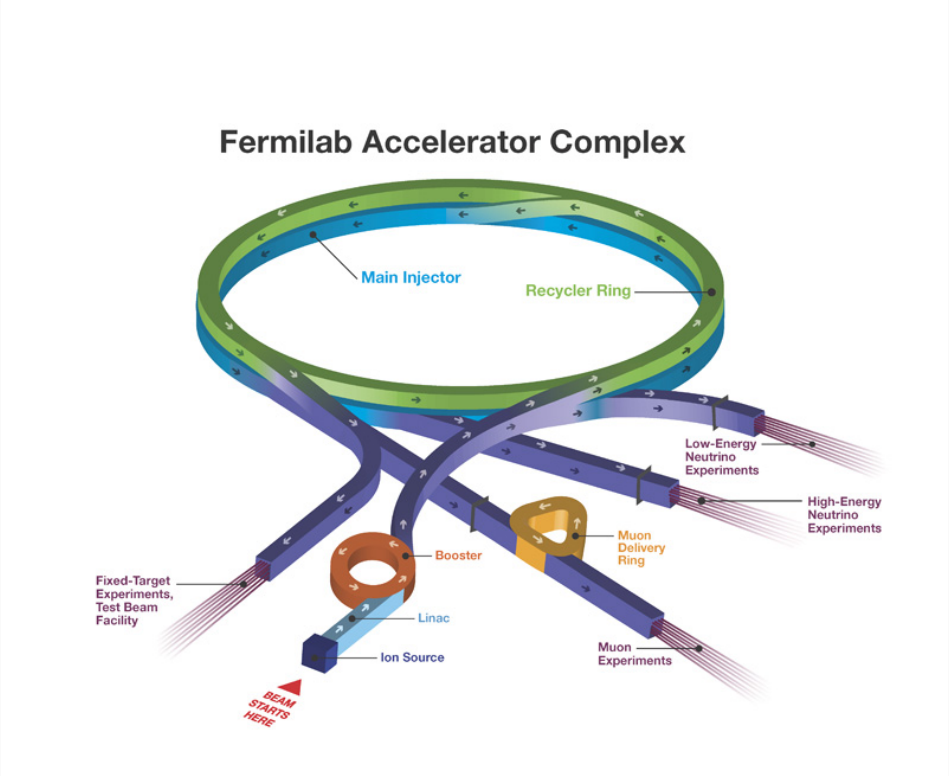

Figure 3: The Fermilab accelerator complex

E989 Contd.

- Protons are accelerated in the linear accelerator Linac to 400 MeV and injected into the Booster, which accelerates protons to 8 GeV.
- The Recycler groups the protons into bunches with approximately 4×10^{12} particles and a temporal width of $\simeq$ 120 ns.
- Each bunch propagates to the AP0 target hall, where protons collide on a cylindrical core made from a nickel-chromium-iron alloy (Inconel-60).
- An electrostatic lithium lens focuses the secondary beam, which then goes through a momentum filter that selects a beam of particles at the magic momentum.
- In the Delivery Ring, spatial separation is created between the pions (together with the emitted muons) and protons, which are more massive and therefore have a smaller Lorentz boost factor given the same momentum. By the time the bunches exit the Ring, they travel $\simeq$ 2km, enough for all pions to decay into muons (decay length $\simeq$ 170m).
- Finally, an inflector magnet cancels the fringe field of the ring itself, which otherwise would deflect the beam into the magnetic iron and reduce injection efficiency.

E989 Contd.

The data from Run 1 and Run 2/3 are as follows [Abi et al. [2021]; Aguillard et al. [2023]]:

$$a_\mu^{exp}(\text{Fermilab, 2021}) = 0.00116592040(54) \rightarrow \pm 0.46\text{ppm}$$
$$a_\mu^{exp}(\text{FermiLab, 2023}) = 0.00116592057(25) \rightarrow \pm 0.21\text{ppm}$$

These data are consistent with the BNL data, with a deviation of 4.2σ, which, although lower than the discovery threshold of 5σ, is still outlier enough for many physicists to consider BSM theories as candidates to solve the mystery.

Hadronic Contributions and Resolution through Lattice

Contributions through strong interactions

- The strong interactions, mediated by gluons also contribute to the magnetic moment
- This contribution is mediated by gluons. We cannot calculate these diagrams perturbatively as QCD is strongly coupled at low energies.
- The first diagram that contributes to the magnetic moment is the hadronic Vacuum Polarization. The contribution is like

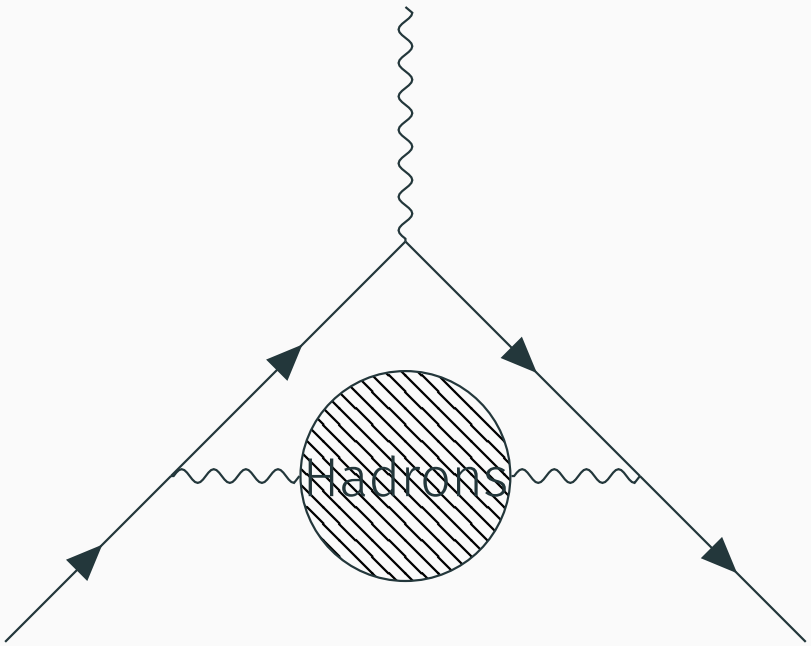

Contd.

- The second contribution is from the Hadronic Light by light Diagram

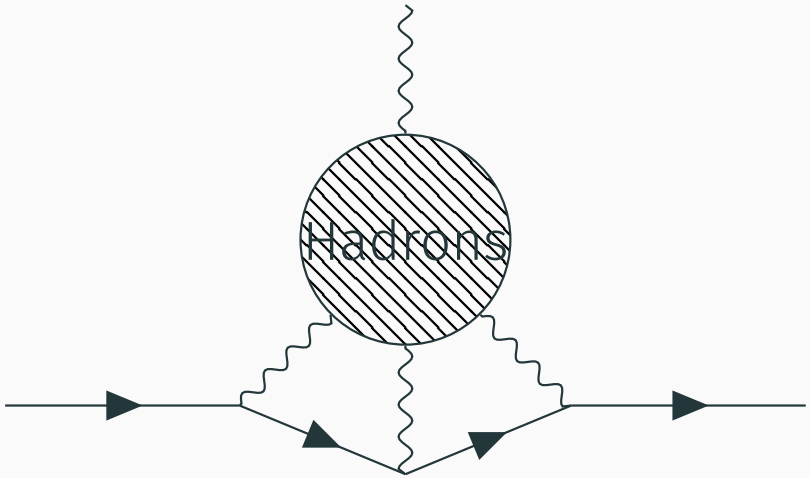

- The contribution of HlBL is very small compared to HVP, so we only discuss the methods to calculate HVP.

Hadronic Vacuum Polarization

- The 1961 paper by Claude Bouchiat and Louis Michel sketches a method to estimate the contribution of Hadronic Vaccum Polarization to the muon's anamolous magnetic moment.
- In particular,they use the cross sections of electron positron scattering to form hadrons to estimate the contribution of HVP.
- Current research uses the methods used by Claude Bouchiat and Louis Michel(Data driven estimation) and lattice QCD to estimate the contribution of HVP.

The Data Diven Approach

- We look first, at the data driven approach.
- In the data driven approach, we use the formula

$$a_\mu^{\text{HVP}} = \left(\frac{\alpha m_\mu}{3\pi}\right)^2 \int_{4m_\pi^2}^{\infty} \frac{ds}{s^2}\, K(s)\, R(s)$$

- Here s is the momentum carried by the photon in the loop in the one loop calculation of g
- The data of cross section of $e^+e^- \to hadrons$ and $e^+e^- \to \mu^+\mu^-$ are used in this method of estimating the contribution HVP.

The structure of Hadron Contribution

- The calculation of the contribution of hadrons starts by looking at the modified photon propagator with hadronic loops.
- The photon propagator before the introduction of hadrons is

$$-\frac{g_{\mu\nu}}{q^2}$$

- The hadron blob contributes through a tensorial term $\Pi(Q)_{\mu\nu}$.
- As the hadron blob is inside a photon propagator, it must obey ward identity,

$$q^{\mu}\Pi(Q)_{\mu\nu} = 0$$

- This restricts $\Pi(Q)_{\mu\nu}$ to be of the form

$$(-Qg_{\mu\nu} + Q_{\mu}Q_{\nu})\Pi(Q^2)$$

Modified virtual photon

- Considering Hadronic contributions, the xact propagator is obtained from a geometric series to be

$$D(Q) = \frac{D^{(0)}}{1 - \Pi(Q^2)}$$

- We next try to write $\Pi(Q^2)$ using an integral by using Cauchy's integral formula.
- This yields us with:

$$\Pi(q^2) = \frac{1}{\pi} \int_{s_0}^{\infty} ds \, \frac{\operatorname{Im} \Pi(s)}{s - q^2 - i\epsilon}$$

Estimating $\Pi(Q^2)$

- The value of $\Pi(Q^2)$ diverges for large Q, so we instead use the integral formula for Π/Q^2
- Using this, we get

$$\Pi(q^2) = \frac{q^2}{\pi} \int_{s_0}^{\infty} ds \, \frac{\mathrm{Im}\,\Pi(s)}{s(s - q^2 - i\epsilon)}$$

- The optical theorem states that the imaginary part of the forward scattering amplitude is related to the total cross-section for producing all possible final states.
- In our case the scattering in question is $\gamma* \to \gamma*$ and the intermediate states are the hadrons.

Optical Theorem

- production of Hadrons from virtual photons is seen in $e^+e^- \to hadrons$.
- So, we can use the scattering amplitude of $e^+e^- \to hadrons$ with appropriate normalization to get $\Pi(Q^2)$

$$Im\Pi(Q^2) = \frac{\alpha}{3} R(Q^2)$$

Where

$$R(Q^2) = \frac{e^+e^- \to hadrons}{e^+e^- \to \mu^+\mu^-}$$

Contribution to the moment

- Now, if have for the free photon, the value of a^μ to be

$$a_\mu \sim \int \frac{d^4q}{(2\pi)^4} \frac{1}{q^2} \times F(q^2, m_\mu)$$

- We take a taylor expansion in $\Pi(q^2)$ to now get

$$a_\mu^{\text{HVP}} \sim \int \frac{d^4q}{(2\pi)^4} \frac{1}{q^2} \Pi(q^2) \times F(q^2, m_\mu)$$

- From this, inserting the value of $\Pi(Q^2)$ we get

$$a_\mu^{\text{HVP}} = \int \frac{d^4q}{(2\pi)^4} \left[\int ds \frac{\text{Im}\,\Pi(s)}{s(s-q^2)} \right] \times F(q^2, m_\mu)$$

- Rewriting the fermion part and Π in terms of K(s) and R(s) the commonly quoted formula is

$$a_\mu^{\text{HVP}} = \left(\frac{\alpha m_\mu}{3\pi} \right)^2 \int_{s_0}^{\infty} \frac{ds}{s^2} K(s) R(s)$$

Data from Data Driven Approach

Contribution	Value $\times 10^{11}$
Experiment (E821)	116 592 089(63)
Experiment (FNAL)	116 592 040(54)
Experiment (World-Average)	116 592 061(41)
HVP LO (e^+e^-)	6931(40)
HVP NLO (e^+e^-)	−98.3(7)
HVP NNLO (e^+e^-)	12.4(1)
HVP LO (lattice, *udsc*)	7116(184)
HLbL (phenomenology)	92(19)
HLbL NLO (phenomenology)	2(1)
HLbL (lattice, *uds*)	79(35)
HLbL (phenomenology + lattice)	90(17)
QED	116 584 718.931(104)
Electroweak	153.6(1.0)
HVP (e^+e^-, LO + NLO + NNLO)	6845(40)
HLbL (phenomenology + lattice + NLO)	92(18)
Total SM Value	116 591 810(43)
Difference: $\Delta a_\mu := a_\mu^{\text{exp}} - a_\mu^{\text{SM}}$	251(59)

Figure 4: Magnetic moment Values for HVP

The Approach of Lattice QCD

- The value of $\Pi(Q^2)$ can also be evaluated on the lattice.
- We first begin by identifying $\Pi_{\mu\nu}$ with the vector current of the quark photon vertex.
- The correlator for the vertex in the position space is given by

$$C_{\mu\nu}^{(N_f)}(x) = \left\langle j_\mu^{(N_f)}(x) j_\nu^{(N_f)}(0) \right\rangle$$

- We use this to get

$$\Pi_{\mu\nu}^{(N_f)}(Q) = \int d^4x \, e^{iQ\cdot x} C_{\mu\nu}^{(N_f)}(x)$$

The calculation

- The calculation of the HVP is now similar to the data driven approach. We integrate using a weight function(kernel) to get the anomalous magnetic moment

$$a_\mu^{\text{HVP, LO}} = \left(\frac{\alpha}{\pi}\right)^2 \int_0^\infty dQ^2 f(Q^2)\widehat{\Pi}(Q^2)$$

- Here we have $\widehat{\Pi}(Q^2) \equiv 4\pi^2 \left[\Pi(0) - \Pi(Q^2)\right]$
- and

$$f(Q^2) = \frac{m_\mu^2 Q^2 Z^3(1 - Q^2 Z)}{1 + m_\mu^2 Q^2 Z^2}, \quad Z = -\frac{Q^2 - \sqrt{Q^4 + 4m_\mu^2 Q^2}}{2m_\mu^2 Q^2},$$

Computing the function

- We have that

$$\Pi(Q^2) = \frac{\sum_\mu \Pi_{\mu\mu}}{3Q^2}$$

- The kernel function f(Q^2) peaks at low momenta, about one fourth the mass of the pion.
- The value of $\Pi(Q^2)$ cannot be computed for very low momenta as lattice extensions of about 10fm would be required
- So, we use extrapolation methods to get the values at low momenta from values at higher momenta

Dividing the integral

- We have that

$$
\begin{aligned}
a_\mu^{\text{HVP, LO}} &= I_0 + I_1 + I_2, \\
I_0 &= \left(\frac{\alpha}{\pi}\right)^2 \int_0^{Q^2_{\text{low}}} dQ^2 \, f(Q^2) \times \hat{\Pi}(Q^2), \\
I_1 &= \left(\frac{\alpha}{\pi}\right)^2 \int_{Q^2_{\text{low}}}^{Q^2_{\text{high}}} dQ^2 \, f(Q^2) \times \hat{\Pi}(Q^2), \\
I_2 &= \left(\frac{\alpha}{\pi}\right)^2 \int_{Q^2_{\text{high}}}^{\infty} dQ^2 \, f(Q^2) \times \hat{\Pi}_{\text{pert}}(Q^2)
\end{aligned}
$$

Dividing the integral

- The calculation for momenta above Q_{high} is done using perturbation theory
- Lattice calculations give the value between Q_{low} and Q_{high}
- For the low momentum regime, which gives the highest contribution, we use extrapolation methods
- The first extrapolation method is to use Pade approximations. Pade approximations are given by

$$\Pi_{[N,M]}(Q^2) = \Pi(0) + \frac{\sum_{i=1}^{N} a_i Q^{2i}}{1 + \sum_{i=1}^{M} b_i Q^{2i}}$$

Time Moments

- The next method is the method of time moments.
- We look at the component of the Vacuum Polarization tensor with identical spatial indices with $Q^\mu = (\omega, 0, 0, 0)$. i.e.,

$$\Pi_{kk}(Q) = Q^2 \Pi(Q^2) = \omega^2 \Pi(\omega^2)$$

- We write

$$\omega^2 \Pi(\omega^2) = \int d^4x \, e^{iQ\cdot x} C_{kk}(x) = -\int dx_0 \, e^{i\omega x_0} \mathcal{C}(x_0)$$

with

$$\mathcal{C}(x_0) = -\frac{1}{3} \sum_{k=1}^{3} \int d^3x \, C_{kk}(x)$$

Time moments

- We now write the moments of this integral,

$$G_{2n} \equiv \int_{-\infty}^{\infty} dx_0\, x_0^{2n} \mathcal{C}(x_0) e^{i\omega \cdot x_0} = (-1)^{n+1} \frac{\partial^{2n}}{\partial \omega^{2n}} \left(\omega^2 \Pi(\omega^2)\right)_{\omega=0}$$

- We now write

$$\Pi(Q^2) = \Pi_0 + \sum_{n=1}^{\infty} \Pi_n Q^{2n}$$

  With

$$\Pi_0 = \Pi(0) = -\frac{1}{2} G_2, \quad \Pi_n = \frac{(-1)^{n+1}}{(2n+2)!} G_{2n+2}$$

- These moments can be used for the construction of Pade approximation.

Lattice QCD: An Intro

- What does it mean to calculate the current $C_{\mu\nu}$ on the lattice?
- In lattice QCD, observables are measured by using the path integral formula for correlation functions

$$\langle O(\phi) \rangle = \frac{1}{Z} \int D\phi \, O(\phi) \, e^{-S(\phi)}$$

- The measure of the path integral is changed to integral over all configurations of the field. The fermion fields live on the sites and the gauge fields live on the links connecting the sites.

Monte Carlo methods

- The average is taken over Lattices generated by $Monte\ Carlo\ Methods$.
- In Monte Carlo methods, we generate configurations with the probability of a configuration being generated given by e^{-S} factor.
- We start the Monte Carlo simulation at a simple configuration like all the links being Unity.
- We then propose new configurations and the Monte Carlo algorithm decides whether or not to accept the proposal.
- **Detailed Balance** ensures that after many Monte Carlo iterations, the probability of a configuration being generated is the equilibrium probability.

Detailed balance and algorithms

- Detailed Balance: If the rate of acceptance to go to a configuration B from a configuration A is $R(A \to B)$ and the equilibrium probability of configuration A is P(A) then

$$R(A \to B)P(A) = R(B \to A)P(B)$$

- The ways in which different Monte Carlo methods do this are
  1. Metropolis: $R(A \to B) = 1$ if P(B)>P(A) and $R(A \to B) = P(B)/P(A)$ if P(B)<P(A)
  2. Heat Bath : $R(A \to B) = P(B)$
- We first do several Monte Carlo steps to reach equilibrium, then do the measurement of observables after intervals of few Monte Carlo steps.

Lattice and Phenomenological Results for $a_\mu^{\text{HVP, LO}}$

Summary of recent lattice and phenomenological results for $a_\mu^{\text{HVP, LO}}$.

Collaboration	N_f	$a_\mu^{\text{HVP, LO}} \times 10^{10}$	Fermion	$\hat{\Pi}(Q^2)$
ETM-18/19	2+1+1	692.1(16.3)	tmQCD	TMR
FHM-19	2+1+1	699(15)	HISQ	Padé w. Moments/TMR
BMW-17	2+1+1	711.1(7.5)(17.5)	Stout4S	TMR
HPQCD-16	2+1+1	667(16)(13)	HISQ	Padé w. Moments
ETM-13	2+1+1	674(21)(18)*	tmQCD	VMD
Mainz/CLS-19	2+1	720.0(12.4)(9.0)	Clover	TMR
PACS-19	2+1	$737(9)^{+13}_{-8}$	StoutW	TMR/Padé
RBC/UKQCD-18	2+1	717.4(16.3)(9.2)	DWF	TMR
Mainz-17	2	$654(32)^{(+21)}_{(-23)}$	Clover	TMR
KNT-19	pheno.	692.8(2.4)	–	dispersion
DHMZ-19	pheno.	694.0(4.0)	–	dispersion
BDJ-19	pheno.	687.1(3.0)	–	dispersion
FJ-17	pheno.	688.1(4.1)	–	dispersion
RBC/UKQCD-18	lat.+pheno.	692.5(1.4)(2.3)	DWF	TMR + disp.

Data for lattice calculations

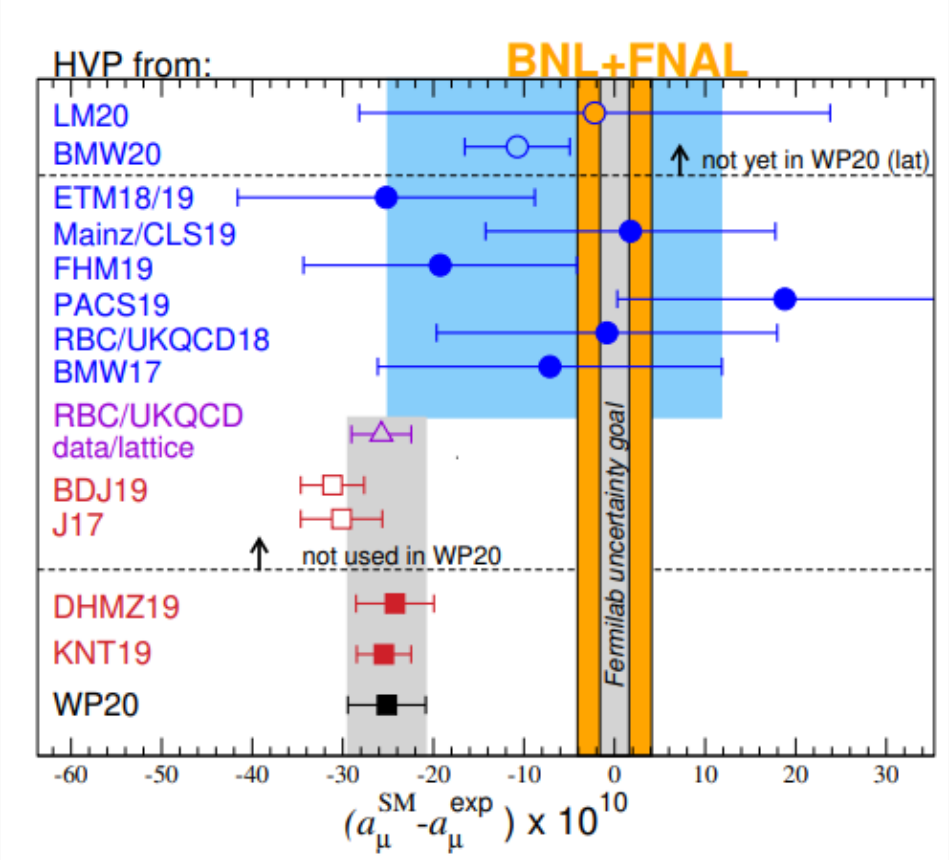

Figure 5: Magnetic moment Values for HVP

The Future: The J-PARC experiment

Future

- Runs 4/5/6 of the E989 experiment aim to improve the precision (now 0.20 ppm) by a factor of 4.
- The upcoming experiment E34 at J-PARC is a completely new setup, doing away with electric fields, and will instead produce muoniums
- These give low energy muons which can be stored using just magnetic fields.
- As there are no electric fields, the only contribution to angular momentum is from the muon's dipole moment, so we can measure the dipole moment of the muon in this experiment.

Muon production and cooling

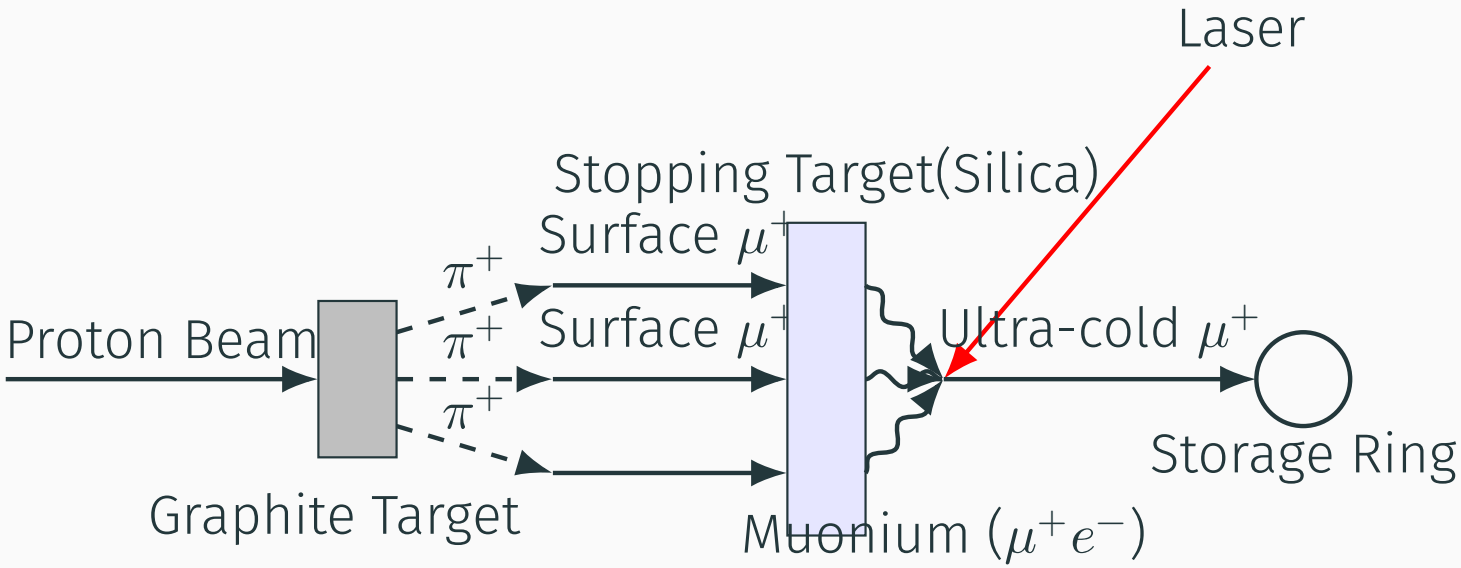

Figure 6: Muon production and cooling at J-PARC.

Muon Production and cooling

- Step 1: protons hit a graphite target. Pions produced come to rest on the graphite.
- Step 2: The pions at rest form surface muons of very low energy.(thermalized)
- Step3: The surface muons go into a silica gel, form muonium
- Step 4: The muonium is excited by laser, muons are accelerated and sent to the storage ring.

The Energies involved

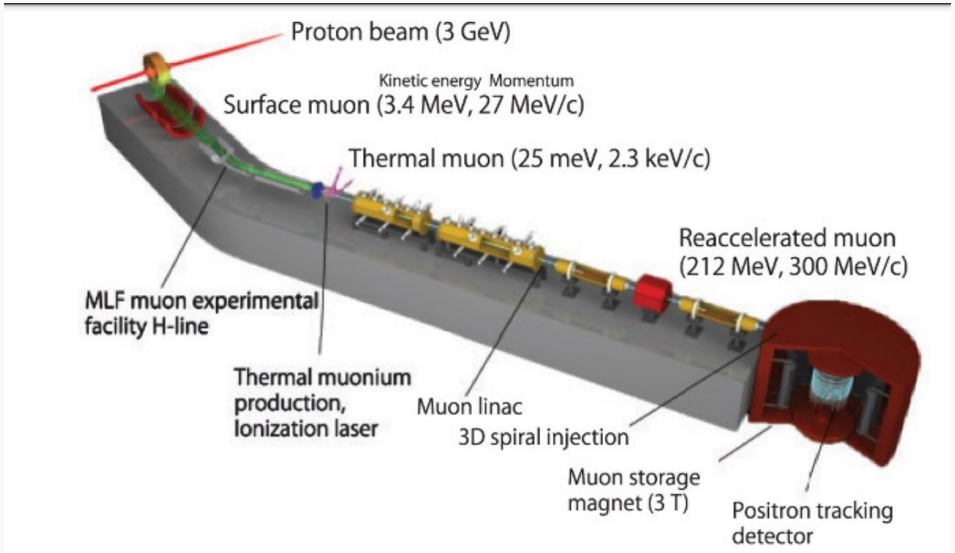

Figure 7: Schematic of energies at JPARC

For comparison, the magic momentum used at BrookHaven and FermiLab is 3.094Gev/c, with the Energy being 3.096GeV

Conclusion

Theoretical Predictions

Table 1: Standard Model Predictions (the brackets represent lattice evaluations)

Contribution	Value $\times 10^{11}$	Error $\times 10^{11}$
QED incl. 4-loops + 5-loops	116 584 718.931	104
Weak to 2-loops	153.6	1.0
Hadronic vacuum polarization	6845	40
Hadronic light-by-light	92	18
Theory	116 591 810	43

Experimental Summary

Table 2: Summary of experiments measuring the muon anomalous magnetic moment.

Experiment	Particles	$a_\mu \times 10^{11}$	Precision [ppm]
CERN I	μ^+	$1162(5) \times 10^5$	4300
CERN II	μ^+, μ^-	$116616(31) \times 10^3$	270
CERN III	μ^+, μ^-	$116592400(850)$	7.3
BNL	μ^+, μ^-	$116592080(63)$	0.54
FNAL	μ^+	$116592055(24)$	0.20
Average (BNL + FNAL)		$116592059(22)$	0.19

References

B. Abi, T. Albahri, S. Al-Kilani, D. Allspach, L. P. Alonzi, A. Anastasi, A. Anisenkov, F. Azfar, K. Badgley, S. Baeßler, I. Bailey, V. A. Baranov, E. Barlas-Yucel, T. Barrett, E. Barzi, A. Basti, F. Bedeschi, A. Behnke, M. Berz, M. Bhattacharya, H. P. Binney, R. Bjorkquist, P. Bloom, J. Bono, E. Bottalico, T. Bowcock, D. Boyden, G. Cantatore, R. M. Carey, J. Carroll, B. C. K. Casey, D. Cauz, S. Ceravolo, R. Chakraborty, S. P. Chang, A. Chapelain, S. Chappa, S. Charity, R. Chislett, J. Choi, Z. Chu, T. E. Chupp, M. E. Convery, A. Conway, G. Corradi, S. Corrodi, L. Cotrozzi, J. D. Crnkovic, S. Dabagov, P. M. De Lurgio, P. T. Debevec, S. Di Falco, P. Di Meo, G. Di Sciascio, R. Di Stefano, B. Drendel, A. Driutti, V. N. Duginov, M. Eads, N. Eggert, A. Epps, J. Esquivel, M. Farooq, R. Fatemi, C. Ferrari, M. Fertl, A. Fiedler, A. T. Fienberg, A. Fioretti, D. Flay, S. B. Foster, H. Friedsam, E. Frlež, N. S. Froemming, J. Fry, C. Fu, C. Gabbanini, M. D. Galati, S. Ganguly, A. Garcia, D. E. Gastler, J. George, L. K. Gibbons, A. Gioiosa, K. L. Giovanetti, P. Girotti, W. Gohn, T. Gorringe, J. Grange, S. Grant, F. Gray, S. Haciomeroglu, D. Hahn, T. Halewood-Leagas, D. Hampai, F. Han, E. Hazen, J. Hempstead, S. Henry, A. T. Herrod, D. W. Hertzog, G. Hesketh, A. Hibbert, Z. Hodge, J. L. Holzbauer, K. W. Hong, R. Hong, M. Iacovacci, M. Incagli, C. Johnstone, J. A. Johnstone, P. Kammel, M. Kargiantoulakis, M. Karuza, J. Kaspar, D. Kawall, L. Kelton, A. Keshavarzi, D. Kessler, K. S. Khaw, Z. Khechadoorian, N. V. Khomutov, B. Kiburg, M. Kiburg, O. Kim, S. C. Kim, Y. I. Kim, B. King, N. Kinnaird, M. Korostelev, I. Kourbanis, E. Kraegeloh, V. A. Krylov, A. Kuchibhotla, N. A. Kuchinskiy, K. R. Labe, J. LaBounty, M. Lancaster, M. J. Lee, S. Lee, S. Leo, B. Li, D. Li, L. Li, I. Logashenko, A. Lorente Campos, A. Lucà, G. Lukicov, G. Luo, A. Lusiani, A. L. Lyon, B. MacCoy, R. Madrak, K. Makino, F. Marignetti, S. Mastroianni, S. Maxfield, M. McEvoy, W. Merritt, A. A. Mikhailichenko, J. P. Miller, S. Miozzi, J. P. Morgan, W. M. Morse, J. Mott, E. Motuk, A. Nath, D. Newton, H. Nguyen, M. Oberling, R. Osofsky, J.-F. Ostiguy, S. Park, G. Pauletta, G. M. Piacentino, R. N. Pilato, K. T. Pitts, B. Plaster, D. Počanić, N. Pohlman, C. C. Polly, M. Popovic, J. Price, B. Quinn, N. Raha, S. Ramachandran, E. Ramberg, N. T. Rider, J. L. Ritchie, B. L. Roberts, D. L. Rubin, L. Santi, D. Sathyan, H. Schellman, C. Schlesier, A. Schreckenberger, Y. K. Semertzidis, Y. M. Shatunov, D. Shemyakin, M. Shenk, D. Sim, M. W. Smith, A. Smith, A. K. Soha, M. Sorbara, D. Stöckinger, J. Stapleton, D. Still, C. Stoughton, D. Stratakis, C. Strohman, T. Stuttard, H. E. Swanson, G. Sweetmore, D. A. Sweigart, M. J. Syphers, D. A. Tarazona, T. Teubner, A. E. Tewsley-Booth, K. Thomson, V. Tishchenko, N. H. Tran, W. Turner, E. Valetov, D. Vasilkova, G. Venanzoni, V. P. Volnykh, T. Walton, M. Warren, A. Weisskopf, L. Welty-Rieger, M. Whitley, P. Winter, A. Wolski, M. Wormald, W. Wu, and C. Yoshikawa. Measurement of the positive muon anomalous magnetic moment to 0.46 ppm. *Phys. Rev. Lett.*, 126:141801, Apr 2021. doi: 10.1103/PhysRevLett.126.141801. URL https://link.aps.org/doi/10.1103/PhysRevLett.126.141801.

Bibliography

D. P. Aguillard, T. Albahri, D. Allspach, A. Anisenkov, K. Badgley, S. Baeßler, I. Bailey, L. Bailey, V. A. Baranov, E. Barlas-Yucel, T. Barrett, E. Barzi, F. Bedeschi, M. Berz, M. Bhattacharya, H. P. Binney, P. Bloom, J. Bono, E. Bottalico, T. Bowcock, S. Braun, M. Bressler, G. Cantatore, R. M. Carey, B. C. K. Casey, D. Cauz, R. Chakraborty, A. Chapelain, S. Chappa, S. Charity, C. Chen, M. Cheng, R. Chislett, Z. Chu, T. E. Chupp, C. Claessens, M. E. Convery, S. Corrodi, L. Cotrozzi, J. D. Crnkovic, S. Dabagov, P. T. Debevec, S. Di Falco, G. Di Sciascio, B. Drendel, A. Driutti, V. N. Duginov, M. Eads, A. Edmonds, J. Esquivel, M. Farooq, R. Fatemi, C. Ferrari, M. Fertl, A. T. Fienberg, A. Fioretti, D. Flay, S. B. Foster, H. Friedsam, N. S. Froemming, C. Gabbanini, I. Gaines, M. D. Galati, S. Ganguly, A. Garcia, J. George, L. K. Gibbons, A. Gioiosa, K. L. Giovanetti, P. Girotti, W. Gohn, L. Goodenough, T. Gorringe, J. Grange, S. Grant, F. Gray, S. Haciomeroglu, T. Halewood-Leagas, D. Hampai, F. Han, J. Hempstead, D. W. Hertzog, G. Hesketh, E. Hess, A. Hibbert, Z. Hodge, K. W. Hong, R. Hong, T. Hu, Y. Hu, M. Iacovacci, M. Incagli, P. Kammel, M. Kargiantoulakis, M. Karuza, J. Kaspar, D. Kawall, L. Kelton, A. Keshavarzi, D. S. Kessler, K. S. Khaw, Z. Khechadoorian, N. V. Khomutov, B. Kiburg, M. Kiburg, O. Kim, N. Kinnaird, E. Kraegeloh, V. A. Krylov, N. A. Kuchinskiy, K. R. Labe, J. LaBounty, M. Lancaster, S. Lee, B. Li, D. Li, L. Li, I. Logashenko, A. Lorente Campos, Z. Lu, A. Lucà, G. Lukicov, A. Lusiani, A. L. Lyon, B. MacCoy, R. Madrak, K. Makino, S. Mastroianni, J. P. Miller, S. Miozzi, B. Mitra, J. P. Morgan, W. M. Morse, J. Mott, A. Nath, J. K. Ng, H. Nguyen, Y. Oksuzian, Z. Omarov, R. Osofsky, S. Park, G. Pauletta, G. M. Piacentino, R. N. Pilato, K. T. Pitts, B. Plaster, D. Počanić, N. Pohlman, C. C. Polly, J. Price, B. Quinn, M. U. H. Qureshi, S. Ramachandran, E. Ramberg, R. Reimann, B. L. Roberts, D. L. Rubin, L. Santi, C. Schlesier, A. Schreckenberger, Y. K. Semertzidis, D. Shemyakin, M. Sorbara, D. Stöckinger, J. Stapleton, D. Still, C. Stoughton, D. Stratakis, H. E. Swanson, G. Sweetmore, D. A. Sweigart, M. J. Syphers, D. A. Tarazona, T. Teubner, A. E. Tewsley-Booth, V. Tishchenko, N. H. Tran, W. Turner, E. Valetov, D. Vasilkova, G. Venanzoni, V. P. Volnykh, T. Walton, A. Weisskopf, L. Welty-Rieger, P. Winter, Y. Wu, B. Yu, M. Yucel, Y. Zeng, and C. Zhang. Measurement of the positive muon anomalous magnetic moment to 0.20 ppm. *Phys. Rev. Lett.*, 131:161802, Oct 2023. doi: 10.1103/PhysRevLett.131.161802. URL https://link.aps.org/doi/10.1103/PhysRevLett.131.161802.

T. Aoyama, M. Hayakawa, T. Kinoshita, and M. Nio. Tenth-Order QED Contribution to the Electron g-2 and an Improved Value of the Fine Structure Constant. *Phys. Rev. Lett.*, 109:111807, 2012. doi: 10.1103/PhysRevLett.109.111807.

J. Bailey, W. Bartl, G. Von Bochmann, R. Brown, F. Farley, H. Jöstlein, E. Picasso, and R. Williams. Precision measurement of the anomalous magnetic moment of the muon. *Physics Letters B*, 28(4):287–290, 1968. ISSN 0370-2693. doi: https://doi.org/10.1016/0370-2693(68)90261-X. URL https://www.sciencedirect.com/science/article/pii/037026936890261X.

J. Bailey, K. Borer, F. Combley, H. Drumm, C. Eck, F. Farley, J. Field, W. Flegel, P. Hattersley, F. Krienen, F. Lange, G. Petrucci, E. Picasso, H. Pizer, O. Runolfsson, R. Williams, and S. Wojcicki. New measurement of (g-2) of the muon. *Physics Letters B*, 55(4):420–424, 1975. ISSN 0370-2693. doi: https://doi.org/10.1016/0370-2693(75)90374-3. URL https://www.sciencedirect.com/science/article/pii/0370269375903743.

Bibliography

G. W. Bennett, B. Bousquet, H. N. Brown, G. Bunce, R. M. Carey, P. Cushman, G. T. Danby, P. T. Debevec, M. Deile, H. Deng, W. Deninger, S. K. Dhawan, V. P. Druzhinin, L. Duong, E. Efstathiadis, F. J. M. Farley, G. V. Fedotovich, S. Giron, F. E. Gray, D. Grigoriev, M. Grosse-Perdekamp, A. Grossmann, M. F. Hare, D. W. Hertzog, X. Huang, V. W. Hughes, M. Iwasaki, K. Jungmann, D. Kawall, M. Kawamura, B. I. Khazin, J. Kindem, F. Krienen, I. Kronkvist, A. Lam, R. Larsen, Y. Y. Lee, I. Logashenko, R. McNabb, W. Meng, J. Mi, J. P. Miller, Y. Mizumachi, W. M. Morse, D. Nikas, C. J. G. Onderwater, Y. Orlov, C. S. Özben, J. M. Paley, Q. Peng, C. C. Polly, J. Pretz, R. Prigl, G. zu Putlitz, T. Qian, S. I. Redin, O. Rind, B. L. Roberts, N. Ryskulov, S. Sedykh, Y. K. Semertzidis, P. Shagin, Y. M. Shatunov, E. P. Sichtermann, E. Solodov, M. Sossong, A. Steinmetz, L. R. Sulak, C. Timmermans, A. Trofimov, D. Urner, P. von Walter, D. Warburton, D. Winn, A. Yamamoto, and D. Zimmerman. Final report of the e821 muon anomalous magnetic moment measurement at bnl. *Phys. Rev. D*, 73:072003, Apr 2006. doi: 10.1103/PhysRevD.73.072003. URL https://link.aps.org/doi/10.1103/PhysRevD.73.072003.

M. Chakraborti, S. Heinemeyer, and I. Saha. The new "MUON G-2" result and supersymmetry. *Eur. Phys. J. C*, 81(12):1114, 2021. doi: 10.1140/epjc/s10052-021-09900-4.

G. Charpak, F. J. M. Farley, R. L. Garwin, T. Muller, J. C. Sens, V. L. Telegdi, and A. Zichichi. Measurement of the anomalous magnetic moment of the muon. *Phys. Rev. Lett.*, 6:128–132, Feb 1961. doi: 10.1103/PhysRevLett.6.128. URL https://link.aps.org/doi/10.1103/PhysRevLett.6.128.

L. Cotrozzi. *Measurement of the muon anomalous precession frequency with the Run-2/3 data in the Muon $g-2$ experiment at Fermilab*. PhD thesis, Pisa U., 3 2024.

J. L. Evans. Effect of ultralight dark matter on $g-2$ of the electron. *Phys. Rev. Lett.*, 132:091801, Feb 2024. doi: 10.1103/PhysRevLett.132.091801. URL https://link.aps.org/doi/10.1103/PhysRevLett.132.091801.

X. Fan, T. G. Myers, B. A. D. Sukra, and G. Gabrielse. Measurement of the Electron Magnetic Moment. *Phys. Rev. Lett.*, 130(7):071801, 2023. doi: 10.1103/PhysRevLett.130.071801.

R. L. Garwin, L. M. Lederman, and M. Weinrich. Observations of the failure of conservation of parity and charge conjugation in meson decays: the magnetic moment of the free muon. *Phys. Rev.*, 105:1415–1417, Feb 1957. doi: 10.1103/PhysRev.105.1415. URL https://link.aps.org/doi/10.1103/PhysRev.105.1415.

C. Gnendiger, D. Stöckinger, and H. Stöckinger-Kim. The electroweak contributions to $(g-2)_\mu$ after the Higgs boson mass measurement. *Phys. Rev. D*, 88: 053005, 2013. doi: 10.1103/PhysRevD.88.053005.

D. Hooper, J. Iguaz Juan, and P. D. Serpico. Signals of a new gauge boson from IceCube and the muon g-2. *Phys. Rev. D*, 108(2):023007, 2023. doi: 10.1103/PhysRevD.108.023007.

F. Jegerlehner. *The Anomalous Magnetic Moment of the Muon*, volume 274. Springer, Cham, 2017. doi: 10.1007/978-3-319-63577-4.

F. Jegerlehner and A. Nyffeler. The Muon g-2. *Phys. Rept.*, 477:1–110, 2009. doi: 10.1016/j.physrep.2009.04.003.

Bibliography

M. Kachelriess. *Quantum Fields — From the Hubble to the Planck Scale*. Oxford University Press, 10 2022. ISBN 978-0-19-287349-1, 978-0-19-880287-7.

S. Navas et al. Review of particle physics. *Phys. Rev. D*, 110(3):030001, 2024. doi: 10.1103/PhysRevD.110.030001.

G. Schneider et al. Double-trap measurement of the proton magnetic moment at 0.3 parts per billion precision. *Science*, 358(6366):1081–1084, 2017. doi: 10.1126/science.aan0207.

M. D. Schwartz. *Quantum Field Theory and the Standard Model*. Cambridge University Press, 3 2014. ISBN 978-1-107-03473-0, 978-1-107-03473-0.

S. Xu and S. Zheng. Resolving muon g-2 anomaly with partial compositeness. *Eur. Phys. J. C*, 82(10):969, 2022. doi: 10.1140/epjc/s10052-022-10949-y.